Extremely high energy ($E > 10^{20}$ eV) cosmic rays: observations and potential sources

Roman Hnatyk[a] and Vadym Voitsekhovskyi[a,*]

[a]*Taras Shevchenko National University of Kyiv, Astronomical Observatory*
Observatorna st. 3, Kyiv, Ukraine

E-mail: roman_hnatyk@ukr.net, v.v.voitsekhovskyi@gmail.com

The search for sources of ultra-high energy cosmic rays (UHECR, $E > 10^{18}$ eV) remains one of the advanced tasks in the high energy astrophysics. The observed high degree of isotropy of the UHECR intensity due to impact of extragalactic and Galactic magnetic fields, together with a significant uncertainty in their chemical composition (atomic masses) due to indirect detection, don't allow to link observed events to their sources and to establish acceleration mechanisms. To reduce the effects of deflection in magnetic fields and composition uncertainty, we consider the most energetic tail of UHECR - rare extremely high energy cosmic rays (EHECR, $E > 10^{20}$ eV). Strongly energy-depended loss length of UHECR - GZK-effect at $E > 10^{19.5}$ eV - further reduces the energy loss horizon of $E > 10^{20.5}$ eV EHECR to a few Mpc level, favoring only protons and Fe group nuclei with ~10 Mpc level. Event-by-event reconstruction of EHECR trajectories in Galactic and extragalactic magnetic fields opens up a possibility to discover their close to us sources. We collect the existing data of EHECR detections at Fly's Eye (1 event), Pierre Auger Observatory (PAO, 14 events after a $k = 1.2$ energy calibration) and Telescope Array (TA, 22 events) and identify their potential sources at distances, restricted by energy loss horizon to 30-50 Mpc, among extragalactic (active galaxy nuclei, starburst galaxies) and Galactic (magnetars) candidates. The most promising candidates are Hypernovae with millisecond pulsar/magnetar, giant flares of magnetars, Kilonovae (NS-NS mergers), tidal disruption events etc. accompanied by (mildly) relativistic jets with close to the Earth directions.

37ᵗʰ International Cosmic Ray Conference (ICRC 2021)
July 12th – 23rd, 2021
Online – Berlin, Germany

---

*Presenter

1. Introduction

In recent years, astronomy is undergoing a revolutionary change – we are witnessing the birth of the gravitational wave astronomy and even more - the birth of the new era of multi-messenger astronomy due to joint observations of gravitational waves, electromagnetic radiation and high-energy neutrinos. Meantime, we are still awaiting for the birth of the cosmic ray astronomy, especially of ultra high energy cosmic ray (UHECR, $E > 10^{18}$ eV) astronomy, responsible for particle physics beyond the Standard Model. The observed high degree of isotropy of the UHECR intensity, caused mainly by deviation of the UHECR trajectories in extragalactic and Galactic magnetic fields, causes the loss of connection to the source. Only at $E > 8$ EeV Pierre Auger Observatory (PAO, Auger) has detected a large-scale dipole anisotropy at the level of 6.5% (statistical significance of 5σ) and UHECR enhancement - PAO Hot Spot - in southern hemisphere, whereas Telescope Array (TA) has detected TA Hot/Cold spot - the 3σ $E > 10^{19.75}$ eV oversampling together with $10^{19.2} < E < 10^{19.75}$ eV event deficit in a circle of $R = 25°$ in the northern hemisphere. Meantime, no signs of significant UHECR excess from potential close sources, including the Virgo Cluster (VC), was found in the TA and Auger data [25]. Only an evidence for cross-correlations (4σ level) with nearby starburst galaxies (SBGs) and $E > 39$ EeV UHECR was found [10]. Significant uncertainty in UHECR chemical composition (atomic masses) of observed events with increasing of heavy element contribution at super-Greizen-Zatsepin-Kuzmin (GZK) $E > E_{GZK} \sim 10^{19.7}$ [15, 32] energies (being inversely proportional to rigidity $R = E/Ze$) further increases trajectories' stochasticity and does not allow to establish UHECR sources and acceleration mechanisms [6]. Considerable reduction of distances to the nearest sources due to EHECR energy losses (GZK suppression via Bethe-Heitler pair production, photo-meson production and nuclei's photo-disintegration) is crucial for the determination of EHECR sources. Analysis of PAO spectrum data shows that the distances to the sources of $E > 10^{19.5}$ eV UHECR, larger than 40(p), 40(He), 70(N), 3(Si), 100(Fe) Mpc for pure elemental p, He, N, Si, Fe compositions, respectively, are rejected at 3σ confidence level [23]. For $E > 10^{20}$ eV UHECR the energy loss horizon is of a few dozen Mpc for H and Fe-group nuclei, and less than 10 Mpc for intermediate mass nuclei [14, 26, 27]. The low EHECR energy loss horizon allows to search for their sources via event-by-event backward trajectory recovering in Galactic and extragalactic magnetic fields, where EHECR propagate in a quasi-ballistic regime. In this work we use the observational data of EHECR detection at Fly's Eye, PAO, and TA for identifying their potential sources at distances up to 30-50 Mpc among extragalactic (active galaxy nuclei (AGN), starburst galaxies (SBGs)) and Galactic (magnetars) candidates.

2. EHECR: observations

At present, the two largest ground-based detectors - PAO and TA - provide UHECR observations. Recently PAO declared 15 events (9 with lg(E/eV)=20.0-20.1 and 6 with lg(E/eV)=20.1-20.2) with $E > 10^{20}$ eV ([3, 4]), and TA declared 22 events [22]. But coordinates of PAO $E > 52$ EeV and zenith angle $\theta < 80°$ UHECR arrival directions (including 6 with $E > 100$ EeV EHECR events) were published back in 2015 [1]. We have been calibrate energies of these events by $k = 1.2$ [27] and obtained 14 calibrated PAO EHECR events (Table 1). List of TA events with $E > 57$

EeV and $\theta < 55°$ from 2008 May 11 to 2013 May 4 includes 10 events with $E > 100$ EeV [5]. Additional 12 events are presented in Fig.5 of [22] and are assigned $E = 10^{20}$ eV energy. New TA sample contains 22 events, including a doublet l = 151°, b = 51° (two events within 1.4° of angular resolution of the TA detector) and a triplet of events in a region 32°< l < 37°, −4.7° < b < 3.3° (a PAO+TA doublet and a TA-event at a distance of 3.7° from it) [22]. The Fly's Eyes event with E = $3.2 \cdot 10^{20}$ eV is also included [8, 12].

Distribution of thus formed EHECR sample on celestial sphere is shown in Fig. 1 together with positions of clusters and superclusters of galaxies, that determine a large-scale mass distribution in the Local Universe (radius ∼ 100 Mpc).
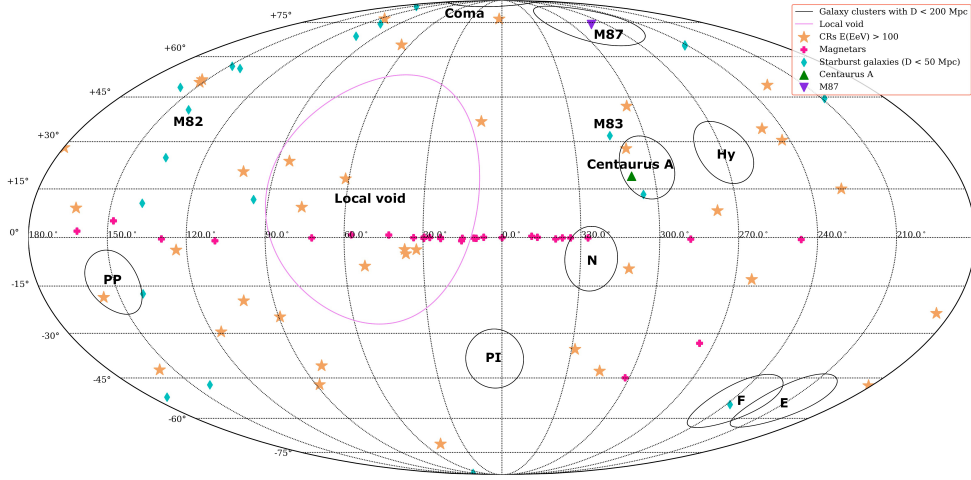
Figure 1: Sky positions of EHECR sample together with positions of some potential sources and clusters/superclusters of galaxies, that determine a large-scale mass distribution in the Local Universe.

3. EHECR: acceleration and propagation effects

The recent list of potential EHECR sources includes a variety of extragalactic objects: AGN, gamma-ray bursts (GRBs), SBGs, newborn millisecond pulsars and magnetars, giant magnetar flares (also observed in our Galaxy), tidal disruption events (TDEs) etc., where permanent/transient jets with high kinetic L_{kin} and magnetic $L_{mag} \lesssim L_{kin}$ luminosities can provide $E > 10^{20}$ eV maximum energies of accelerated particles [24]:

$$\frac{E_{max}}{10^{20}eV} \lesssim \frac{Ze}{10^{20}eV}\left(\frac{L_{kin}\beta}{c\Gamma^2}\right)^{1/2} = 0.1Z\left(\frac{L_{kin}}{10^{45.5}erg/s}\right)^{1/2}\left(\frac{\Gamma^2/\beta}{100}\right)^{-1/2} \tag{1}$$

where $\beta = v/c$ is the dimensionless speed of jet, $\Gamma = 1/(1 - \beta^2)^{1/2}$ is its Lorenz factor.

Furthermore, EHECR from both Galactic and extragalactic sources will move quasi-ballistically, slightly deflecting in magnetic fields and without switching to the diffusion propagation mode. Therefore, to identify their sources, we can use the event-by-event backtracking analysis for comparing a sky position of each detected event with specific astrophysical objects. The average angular

Table 1: List of EHECR events (including triplet (†), doublet (††) and TA events with assigned energy $E = 100$ eV (*))

E	E_{calibr}	RA	Dec	Gal l	Gal b	E	E_{calibr}	RA	Dec	Gal l	Gal b
EeV	EeV	deg	deg	deg	deg	EeV	EeV	deg	deg	deg	deg
PAO											
127.1	152.5	192.8	-21.2	-57.1	41.7	92.8	111.3	343.3	-71.6	-44.9	-42.6
118.3†	141.9	287.7	1.5	36.5	-3.6	89.3	107.1	116	-50.6	-96.4	-12.9
118.3	141.9	340.6	12.0	80.1	-39.9	89.1	106.9	218.8	-70.8	-48.7	-9.7
111.8	134.1	352.6	-20.8	47.5	-70.5	89.0	106.8	349.9	9.3	88.4	-47.3
108.2	129.8	45.6	-1.7	179.5	-49.6	85.3	102.3	123.3	-6.2	-131.7	15.1
100.1	120.1	150.1	-10.3	-110.9	34.1	84.8	101.7	154.5	-46.9	-82.4	8.3
99.0	118.8	309.5	-66.7	-31.5	-35.2	84.7	101.6	199.6	-34.8	-50.8	27.7
TA											
162.2		205	20	3.2	76.4	100*		280	56	85	23
154.3		239.8	-0.4	9.3	36.2	100*		15	59	124	-3
139		152.3	11.1	228.6	49.4	100*		300	13	52	-8
135.3†		288.3	0.3	33.2	-4.1	100*		158	57	152	51
124.8		295.6	43.5	76.4	9.2	100*††		157	58	151	50
122.2		347.7	39.4	101.4	-19.7	100*††		195	40	115	77
120.3		285.4	33.6	63.5	12.3	100*		69	11	185	-23
106.8		37.6	13.9	156.3	-42.7	100*		52	34	156	-18
101.4†		285.7	-1.7	32.6	-3.1	100*		338	29	89	-24
101		219.6	38.5	65.8	64.3	100*		298	70	102	20
100*		118	40	179	28	100*		6	33	116	-29
100*		278	33	61	18	100*		144	-9	243	30
Fly's Eye											
320		85	48	163	9						

EHECR deflection Θ_{rms} and the corresponding time delay τ_{rms} in the random field B_{rms} with the coherence length l_c at the distance L, are following [30, 31]:

$$\Theta_{rms}(E,L) = \sqrt{\frac{2}{9}}\left(\frac{Ze}{E}\right)B_{rms}\sqrt{l_c L} \simeq 0.08°Z\left(\frac{E}{10^{20}\text{eV}}\right)^{-1}\left(\frac{L}{10\text{Mpc}}\right)^{\frac{1}{2}}\left(\frac{l_c}{1\text{Mpc}}\right)^{\frac{1}{2}}\left(\frac{B_{rms}}{10^{-10}\text{G}}\right) \quad (2)$$

and

$$\tau_{rms}(E,L) = L\Theta_{rms}^2(E,L)/4c \simeq 15Z^2\left(\frac{E}{10^{20}eV}\right)^{-2}\left(\frac{L}{10\text{Mpc}}\right)^2\left(\frac{l_c}{1\text{Mpc}}\right)\left(\frac{B_{rms}}{10^{-10}G}\right)^2 \text{yr} \quad (3)$$

Galactic magnetic field is represented by a regular and a random component due to Jansson-Farrar model [20, 21]. The expected order of magnitude for the deflections in random Galactic and extragalactic magnetic fields is $\sim 3°Z(E/100EeV)^{-1}$ [9].

EHECR detection is significantly affected by energy losses, due to interactions with background electromagnetic (CMB and IR) radiation in extragalactic environment. These losses (photodisintegration of heavy nuclei and photo-pion losses of protons dominate at $E > 10^{20}$ eV) significantly restrict EHECR energy loss lengths $\lambda_{loss} = -c(d \ln E/dt)^{-1}$, limiting the distance to potential sources up to ~ 100 Mpc for protons and heavy nuclei (Si, Ca, Fe) and up to ~ 30 Mpc for intermediate nuclei (He, C-N-O) taking into account their secondary origin from photodisintegration of heavy nuclei [13].

4. EHECR: potential sources

The most popular UHECR sources: AGN and GRBs are predominantly at cosmological distances, considerably larger than EHECR energy loss horizon of protons and heavy nuclei $R_h \sim 100$ Mpc. Therefore we include in the list of potential EHECR sources UHECR sources inside Local Universe - up to ~ 100 Mpc. Namely, SBGs with high-velocity ($v > 1000$ km s^{-1}) magnetised ($B_w \sim 1$ mG) galactic winds, ordinary galaxies - potential hosts of Hypernovae with 3% of core collapse SN rate and of Kilonovae (double neutron star merger), as well as Galactic magnetars. All of them can provide $E_{max} \sim 10^{19}Z$ eV EHECR for Z>10 [7, 28].

In our work the arrival directions of EHECR corrected for the influence of Galactic and extragalactic magnetic fields were compared with the samples of active in $\gamma-$ray range AGN and SBGs [2] and of magnetars[1] in our Galaxy and Magellanic Clouds [19, 29].

The results of recovering backward trajectories of $E > 10^{20}$ eV EHECR in Galactic and extragalactic magnetic fields in Local Universe are presented in Table 2 and in Fig. 2. We found out that protonic EHECR (Fig. 2a) are nearly isotropic without clear correlations with potential sources. EHECR with intermediate (Z=6-14) composition (Fig. 2b-2c) are considerably deflecting due to anisotropic nature of Galactic magnetic field lensing and provide increasing of overlapping with SBGs. Heavy nuclei of Fe group (Fig. 2d) are strongly deflected by Galactic magnetic field into extended region $40° < l < 270°$, $b > 0°$ [11]. Considerable overlapping with SBGs are mainly due to spreading of EHECR trajectories. Spread of EHECR trajectories are too large for revealing of potential sources.

Meantime, Galactic magnetars can be promising potential sources of EHECR (Fig. 3a,3b). So, magnetar SGR 1900+14 ($l = 43.02°$, $b = 0.77°$) at a distance of 12.5 ± 1.7 kpc could be the potential source of the triplet [16–19] (Fig.3).

5. Summary

Severe energy losses reduce the energy loss horizon of $E > 10^{20}$ (3×10^{20}) eV sources to $\sim 30 - 50$ ($10 - 20$) Mpc with preference to H and Fe nuclei as the most promising probe for identifying potential sources. Recovering of backward trajectories of observed $E > 10^{20}$ eV EHECR in Galactic and extragalactic magnetic fields in the Local Universe is informative for $Z \lesssim 10$ nuclei and support SBGs as a extragalactic EHECR sources. Z=1-2 (representative value for H-He group) EHECR are weakly deflected by magnetic field, their sky distribution remains nearly isotropic. In two cases (including EHECR doublet) EHECR might be connected with nearby

---

[1]http://www.physics.mcgill.ca/ pulsar/magnetar/main.html

(a) Z=1, 2   **(b)** Z = 6

                                           (c) Z=14   **(d)** Z = 26
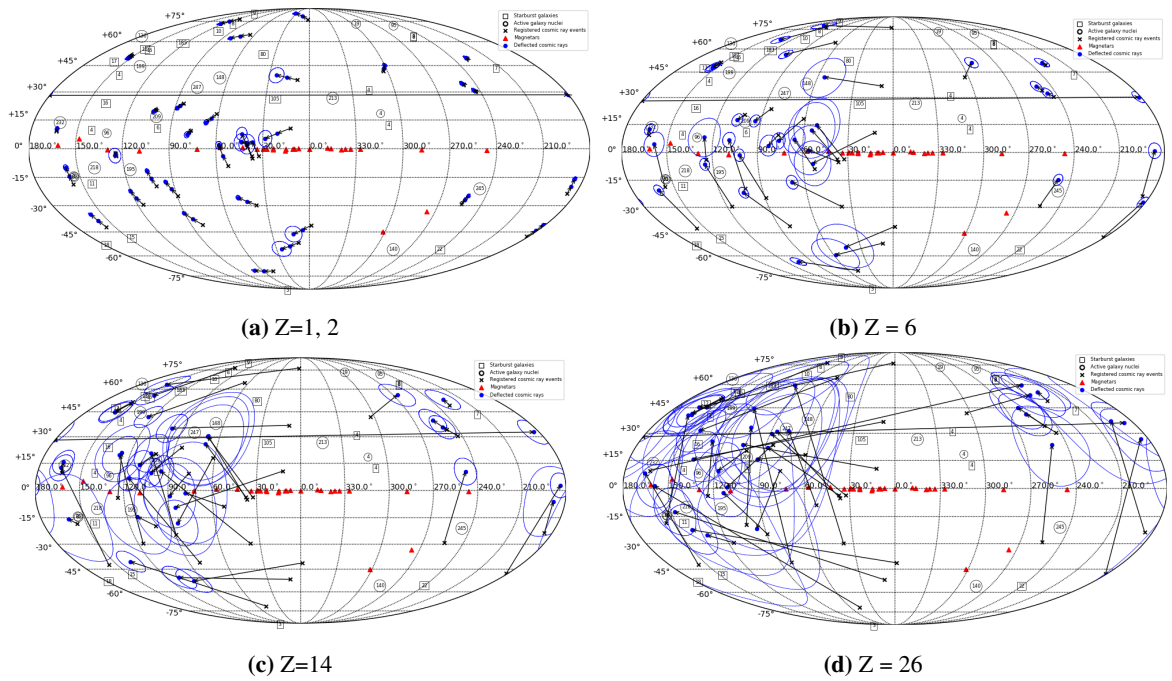
Figure 2: Sky positions of $E > 10^{20}$ eV Z=1,2(a), 6(b), 14(c), 26(d) EHECR, corrected for Galactic and extragalactic (up to 50 Mpc) magnetic field deflection. Observed distribution of EHECR arrival directions (crosses), their recovering distribution at the Galaxy's boundary (tops of arrows) and 1σ circles of total deflection in random Galactic and extragalactic magnetic fields at 50 Mpc, together with potential sources - SBGs (squares), γ-ray active AGN (circles) with indicated distances (in Mpc), and Galatic + Magellanic Clouds magnetars (red triangles) - are presented.

(a)   **(b)**
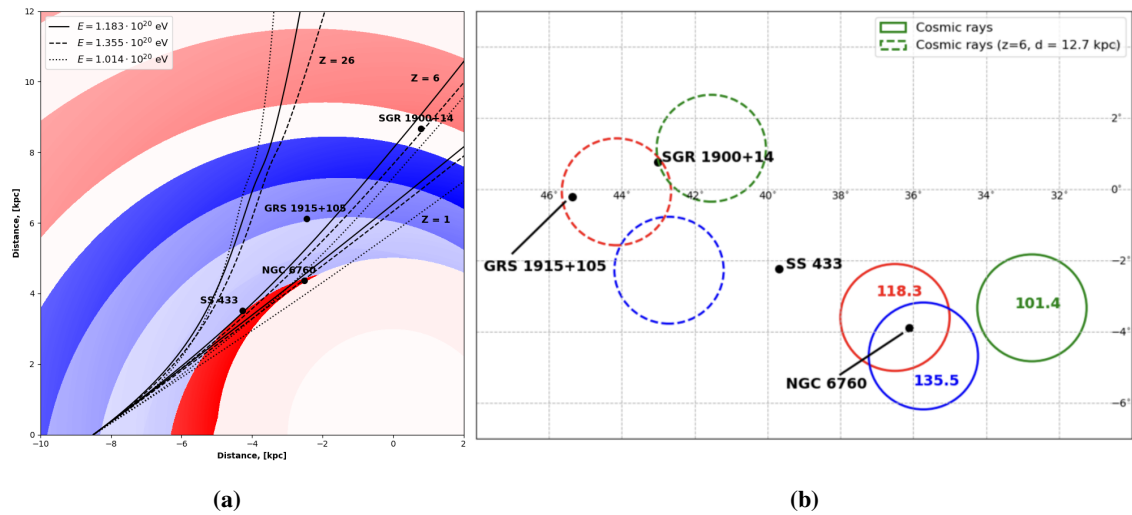
Figure 3: Backward trajectories of EHECR triplet in Galactic magnetic field (a) and their sky position at SGR 1900+14 d = 12.5 kpc distance (b)

Table 2: Potential sources of EHECR

Element	$L_{loss}[Mpc]$ lg(E/eV)=20/20.5/21	Galactic Magnetars	Starburst galaxies
H	20/3.5/5	SGR 1935+2154	NGC5055, 3XMM J185246+003317
He	0.5/2/1	SGR 1900+14	-
N	2/0.1/0.3	4U 0142+61, SGR 0501+4516, SGR 1935+2154, SGR1900+14 3XMM J185246+0033176	NGC5055, NGC4631
Si	50/0.15/0.3	1E2259+586, SGR 2013+34, 4U 0142+61, SGR 0501+4516, SGR 1935+2154	NGC 3079, NGC2146, NGC891, NGC6946, NGC3628, NGC3627
Fe	60/10/0.3	SGR 0418+5729, 4U 0142+61 1E2259+586, SGR 2013+34, SGR 0501+4516, SGR 1935+2154	NGC6946, M51, NGC5055 NGC2146, IC342, NGC891, M82, NGC660, Arp299, NGC4631 NGC3556, NGC3079, NGC1068

SBGs (Fig. 2a). Z=6 EHECR are considerably deflected in the Galaxy plane region, avoiding Galactic centre region. The number of SBGs - potential EHECR sources - increases (Fig. 2b). Z=26 EHECR are strongly deflected, magnetic lensing by Galactic magnetic field strongly increases contribution from extended region $40° < l < 270°$, $b > 0°$ and decreases one from Galactic centre region with increasing of Z [11]. Preferable acceleration mechanisms are shock wave/magnetic field reconnection in transient collimated directed to the Earth jets in rare GRBs, Kilonovae (NS-NS mergers), TDEs and in more frequent Hypernovae with millisecond pulsar/magnetar and giant flares of Galactic and extragalactic magnetars, accompanied by (mildly) relativistic jets with close to the Earth directions. Particularly Galactic magnetar SGR1900+14 may be responsible for the observed EHECR triplet (Fig. 3a,3b).

The next-generation ground-based (AugerPrime, GCOS) and space (POEMMA) detectors will play crucial role in discovering UHECR, especially, EHECR sources.

6. Ackowledgements

References

[1] A. Aab et al., ApJ **794** (2014) 172

[2] A. Aab et al., ApJL **853** (2018) L29

[3] A. Aab et al., Phys. Rev. Lett. **125** (2020) 121106

[4] A. Aab et al., Phys. Rev. D **102** (2020) 062005

[5] R. U. Abbasi et al., ApJL, **790** (2014) L21

[6] L. Anchordoqui, Phys. Rept. **801** (2019) 1

[7] R. A. Batista et al., Front. Astron. Space Sci. **6** (2019) 23

[8] D. J. Bird et al., ApJ, **441** (1995) 144

[9] O. Deligny, PoS ICRC2019 (2019) 234

[10] O. Deligny, Astropart. Phys. **104** (2019) 13

[11] G. Farrar, M. Sutherland, J. Cosmol. Astropart. Phys. **5** (2019) 4

[12] T.Fitoussi, G. Medina-Tanco, J.-C.D'Olivo, PoS ICRC2019 (2019) 256

[13] N. Globus et al., MNRAS **484** (2019) 4167

[14] J.M. Gonz´alez, S.Mollerach and E.Roulet, arXiv:2105.08138v1

[15] K. Greisen, Phys. Rev. Lett., **16** (1966) 748

[16] R. Gnatyk, Kinemat. Phys. Celest. Bodies **32** (2016) 1

[17] R. Gnatyk, Kinemat. Phys. Celest. Bodies **34** (2018) 167

[18] B. Hnatyk, R. Hnatyk, V. Zhdanov, V. Voitsekhovskyi, arXiv:2009.06081

[19] R. Hnatyk, V. Voitsekhovskyi, Kinemat. Phys. Celest. Bodies **36** (2020) 129

[20] R. Jansson, G. Farrar, Astrophys. J. Lett. **761** (2012) L11

[21] R. Jansson, G. Farrar, Astrophys. J. **757** (2012) 14

[22] K. Kawata et al., EPJ Web of Conf. **210** (2019) 01004

[23] R.G.Lang, A. M. Taylor, M. Ahlers, V. de Souza, Phys. Rev. D **102** (2020) 063012

[24] M. Lemoine, E. Waxman, J. Cosmol. Astropart. Phys. **11** (2009) 9

[25] J. Matthews, PoS ICRC2017 (2017) 1096

[26] L. Merten et al., arXiv:2102.01087v1;

[27] M. Muzio, M. Unger, G. R. Farrar, arXiv:1906.06233v2

[28] K. Murase, M. Fukugita, Phys. Rev. D **99** (2019) 6

[29] S.A. Olausen, V. M. Kaspi, ApJ Suppl. **212** (2014) 1

[30] G. Sigl, F. Miniati, T. A. Ensslin, Phys. Rev. D **68** (2003) 043002

[31] E. Waxman, J. Miralda-Escude, ApJ **472** (1996) L89

[32] G. Zatsepin , V. Kuzmin,, J. Exp. Theor. Phys. Lett. **4** (1966) 78